AGU PUBLICATIONS

JGR

Journal of Geophysical Research: Oceans

RESEARCH ARTICLE

10.1002/2017JC013135

Flow Patterns in the Eastern Chukchi Sea: 2010–2015

Phyllis Stabeno[1], Nancy Kachel[1,2], Carol Ladd[1], and Rebecca Woodgate[3]

[1]Ocean Environment Research Division, NOAA Pacific Marine Environmental Laboratory (PMEL), Seattle, Washington, USA, [2]Joint Institute for the Study of the Atmosphere and Ocean (JISAO), University of Washington, Seattle, Washington, USA, [3]Applied Physics Laboratory, University of Washington, Seattle, Washington, USA

Key Points:
- Average annual transport near Icy Cape, AK is ~0.4 Sv accounting for ~40% of the northward flow of Pacific water through Bering Strait
- The transport varies seasonally, accounting for >50% of total transport through Bering Strait in summer and ~20% in winter
- Year-round current (Chukchi Slope Current) flows westward along the north slope of the Chukchi from at least Barrow Canyon to Herald Canyon

Correspondence to:
P. Stabeno,
phyllis.stabeno@noaa.gov

Citation:
Stabeno, P., Kachel, N., Ladd, C., & Woodgate, R. (2018). Flow patterns in the eastern Chukchi Sea: 2010–2015. *Journal of Geophysical Research: Oceans*, *123*, 1177–1195. https://doi.org/10.1002/2017JC013135

Received 25 MAY 2017
Accepted 1 JAN 2018
Accepted article online 8 JAN 2018
Published online 12 FEB 2018

Abstract From 2010 to 2015, moorings were deployed on the northern Chukchi Sea at nine sites. Deployment duration varied from 5 years at a site off Icy Cape to 1 year at a site north of Hanna Shoal. In addition, 39 satellite-tracked drifters (drogue depth 25–30 m) were deployed in the region during 2012–2015. The goals of this manuscript are to describe currents in the Chukchi Sea and their relationship to ice and winds. The north-south pressure gradient results in, on average, a northward flow over the Chukchi shelf, which is modified by local winds. The volume transport near Icy Cape (~0.4 Sv) was ~40% of flow through Bering Strait and varied seasonally, accounting for >50% of summer and ~20% of winter transport in Bering Strait. Current direction was strongly influenced by bathymetry, with northward flow through the Central Channel and eastward flow south of Hanna Shoal. The latter joined the coastal flow exiting the shelf via Barrow Canyon. Drifter trajectories indicated the transit from Bering Strait to the mouth of Barrow Canyon took ~90 days during the ice-free season. Most (~70%) of the drifters turned westward at the mouth of Barrow Canyon and continued westward in the Chukchi Slope Current. This slope flow was largely confined to the upper 300 m, and although it existed year-round, it was strongest in spring and summer. Drifter trajectories indicated that the Chukchi Slope Current extends as far west as the mouth of Herald Canyon. The remaining ~30% of the drifters turned eastward or were intercepted by sea ice.

1. Introduction

The Chukchi Sea consists of a broad shallow shelf, extending >800 km northward from its southern boundary at Bering Strait to the shelf break bounding the Arctic basin. It is characterized as an inflow shelf for the Arctic (Carmack & Wassmann, 2006), with ~1×10^6 m^3 s^{-1} (1 Sv) of Pacific water entering the shelf through Bering Strait (Woodgate et al., 2005a, 2012). Throughout the Chukchi, the annual mean flow through Bering Strait continues generally northward following bathymetry (Woodgate et al., 2005b). Much of this flow exits the Chukchi shelf through two canyons—Barrow (Coachman et al., 1975; Weingartner et al., 2005) in the east and Herald (Coachman et al., 1975; Pickart et al., 2010) in the west. The water entering the Chukchi Sea through Bering Strait is generally classified into three types (Coachman et al., 1975; Danielson et al., 2017; Gong & Pickart, 2015; Woodgate et al., 2005b): seasonally present, warm, fresh Alaskan Coastal Water (ACW); nutrient-rich, colder and saltier Anadyr Water (AW) from the northwestern Bering Sea shelf; and Bering Sea Water (BSW) with intermediate properties primarily from 100 m isobath flow (Stabeno et al., 2016). These water masses provide heat, freshwater (ACW), and salt, including nutrients (BSW, AW), to the Chukchi Sea.

The northward flow through Bering Strait is generally believed to be driven by a Pacific-Arctic pressure head (Aagaard et al., 2006; Stigebrandt, 1984), which forces the mean northward flow through Bering Strait (Kinder et al., 1986). While the annual mean flow is northward, local winds modify the flow, and on time scales of days to weeks can even reverse it (Woodgate et al., 2005b, 2015). In general, the strongest northward flow through the strait occurs in the summer months, while the strong southward winds in winter result in weaker northward monthly averaged flows (see Woodgate et al., 2005a for a climatology).

This paper concentrates on data sets from moorings, satellite-tracked drifters and hydrographic surveys collected from 2010 to 2015 as part of three Bureau of Ocean Energy Management (BOEM) projects: Chukchi Acoustics, Oceanography, and Zooplankton Study (CHAOZ, field years 2010–2012); CHAOZ-Extension (field years 2013–2015); and Arctic Whale Ecology Study (ARCWEST, field years 2013–2015). The goal of these studies was to better understand the Chukchi ecosystem from physics to marine mammals.

The focus of this paper is on a narrow component of the large and diverse data sets collected as part of these three BOEM programs: the flow patterns on the eastern Chukchi shelf. Data and data handling methods are described in section 2. Results are presented in section 3, including: observations on the patterns and strength of the currents; estimates of total transport at Icy Cape; the relationship between winds and currents/transport; and transit times. Section 4 provides a discussion and summary of the results and conclusions.

2. Data and Methods

2.1. Sea Ice

The Advanced Microwave Scanning Radiometer for EOS (AMSR-E) data (available from the National Snow and Ice Data Center, http://nsidc.org/data/amsre/) were used in this manuscript. AMSR is a data set of sea-ice extent and areal concentration consisting of daily ice concentration data at 12.5 km resolution. Time series of percent areal coverage were calculated in 25 km $\times$ 25 km boxes around each of the mooring sites discussed in this manuscript.

2.2. Reanalysis Winds

Wind velocity was obtained from the North American Regional Reanalysis (NARR) and interpolated to the mooring sites. NARR was introduced as an extension to the National Centers for Environmental Prediction (NCEP) Reanalysis 2 (NCEPR2) for the North American Region using the high resolution NCEP Eta model ($\sim$32 km grid size compared to NCEPR2's 2.5° grid) and includes additional assimilated parameters to improve the reanalysis product (Mesinger et al., 2006). NARR winds are available at 3 hourly intervals, and were binned and averaged into 6 hourly intervals for this study.

NCEP winds are well correlated with the observed winds in the Bering Sea (Ladd & Bond, 2002). More recently, the NARR winds have been shown to better resolve coastal winds in the northern Gulf of Alaska ($\sim$60°N; Stabeno et al., 2016).

2.3. Current Measurements

Moorings (Table 1 and Figure 1) were deployed at nine sites (C1–C9) on the Chukchi shelf. To avoid ice keels, each mooring was $<$10 m tall, thus keeping the upper float at least 30 m below the surface. This requirement proved prudent—on 18 April 2011 our ASL ice profiler measured a 29 m keel passing over C1. The oceanographic moorings contained instruments that measured ice thickness, fluorescence (chlorophyll), nitrate, oxygen, photosynthetically active radiation (PAR), temperature, and salinity (SBE16), as well as current speed and direction (Berchok et al., 2015). To include all of these instruments and limit the height of the mooring, at least two moorings were deployed at each site. This paper primarily focuses on the velocity measurements (Table 1). Current measurements were collected on subsurface moorings using acoustic Doppler current profilers (ADCP; Teledyne RD Instruments). A nearby mooring included point current meters (Aanderaa RCM-9, RCM-11). At mooring sites C1–C8 (water depths of 40–50 m), the ADCPs were upward looking and either 300 or 600 kHz. The Aanderaa instruments were deployed within 6 m of the bottom. Mooring C9 was deployed in $\sim$1,000 m of water along the Chukchi slope west of Barrow Canyon. This mooring included three RCM current meters at $\sim$900 m, $\sim$600 m, $\sim$310 m, and an upward looking 75 kHz ADCP at $\sim$300 m. Failure rates for the ADCPs were relatively high, with five out of 23 failing over the years primarily because of interference of bolts holding the ADCP with one of the beams of the ADCP.

Data were collected at least hourly and all instruments were calibrated prior to deployment. The data were processed according to manufacturers' specifications. All current meter time series were low-pass filtered with a 35 h, cosine-squared, tapered Lanczos filter to remove tidal and higher-frequency variability, and resampled at 6 h intervals. Final processed time series data are good to $\pm$0.002°C, $\pm$0.0005 S/m, $\pm$0.5 cm s^{-1} (temperature, salinity, and currents, respectively). At mooring site C2, the drift in the salinity of the moored SBE16 was minimal ($<$0.05) when compared to the CTD data collected at that site.

2.4. Shipboard Hydrography

Each year from 2010 to 2015 hydrographic data were collected along a set of transects during cruises using a Sea-Bird SBE 911plus system. CTD measurements were made using a system with dual temperature, salinity, and dissolved oxygen (SBE-43) sensors, and single chlorophyll fluorescence (WET Labs WETStar WS3S) and PAR (Biospherical Instruments QSP-200 L4S or QSP-2300) sensors. Bottle samples of salinity, chlorophyll,

Table 1
Current Meter Instruments Used in this Paper

Site	Latitude (°N) Longitude (°W)	Depth (m)	Beginning and end of record	Instruments
C1	70.835	44	29 Aug 2010 to 25 Aug 2011	600 kHz
	163.119		25 Aug 2011 to 29 Apr 2012	RCM-9
			27 Aug 2013 to 25 Sep 2014	300 kHz
			25 Sep 2014 to 18 Sep 2015	300 kHz
C2	71.222	43	29 Aug 2010 to 23 Aug 2011	600 kHz
			24 Aug 2011 to 21 Aug 2012	600 kHz
	164.250		22 Aug 2012 to 27 Aug 2013	RCM-9
			27 Aug 2013 to 27 Sep 2014	600 kHz
			27 Sep 2014 to 3 Oct 2015	RCM-9
C3	71.825	45	31 Aug 2010 to 22 Aug 2011	600 kHz
	165.975		26 Aug 2011 to 22 Aug 2012	600 kHz
C4	71.042	51	10 Oct 2014 to 13 Sep 2015	300 kHz
	160.493			
C5	71.207	53	31 Aug 2013 to 29 Sep 2014	300 kHz
	157.999		29 Sep 2014 to 14 Sep 2015	600 kHz
C6	71.777	42	29 Aug 2013 to 7 Oct 2014	600 kHz
	161.875		7 Oct 2014 to 17 Sep 2015	300 kHz
C7	72.424	42	29 Aug 2013 to 2 Oct 2014	600 kHz
	161.604			
C8	72.586	46	3 Oct 2014 to 16 Sep 2015	300 kHz
	161.215			
C9	72.467	950	1 Oct 2014 to 15 Sep 2015	75 kHz, RCM-9 and 11
	156.550			

Note. Depth indicates bottom depth.

oxygen, and nutrients (nitrate, phosphate, silicate, nitrite, and ammonium) were collected for later processing at Pacific Marine Environmental Laboratory (PMEL) in Seattle, Washington. Data were recorded during the downcast, with a descent rate of 15 m min^{-1} to a depth of 30 m, and 30 m min^{-1} below that. Salinity calibration samples were taken on approximately a third of the casts and analyzed on a laboratory salinometer. The primary purpose of the water samples collected for salinity and oxygen was to ensure data quality. Nutrients and chlorophyll samples were collected at the surface, at 10 m intervals throughout the water column, and at the bottom of the cast.

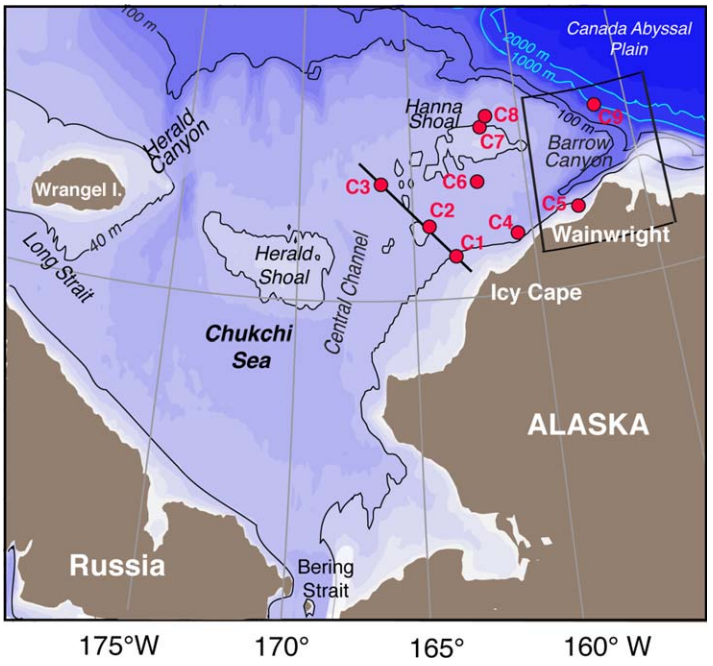

Figure 1. Map of the Chukchi Sea shelf with bathymetry and place names. The nine mooring sites (C1–C9) presented in this paper are indicated in red. Icy Cape line comprises C1, C2, and C3.

2.5. Satellite-Tracked Drifters

Since 2012, 39 satellite-tracked drifters ("holey sock" drogue centered at ~25–30 m) have been deployed in Chukchi Sea by investigators from the EcoFOCI program at PMEL (www.ecofoci.noaa.gov/drifters/efoci_driftersIntro.shtml). In addition to position, each drifter measured sea surface temperature. At these high latitudes, an average of ~14 position fixes per day was obtained from Argos. Data were examined and spurious points were deleted from the time series, as were data collected after the drogue was lost (as indicated by a drifter sensor), the drifter went aground or entered into ice (determined from maps of ice extent). The resulting time series were then linearly interpolated to hourly intervals.

2.6. Calculation of Transport

Estimates of total transport were obtained following the approach previously applied in the Gulf of Alaska (Schumacher et al., 1989; Stabeno et al., 1995, 2016). In this approach, the current data were low-pass filtered and the component of velocity perpendicular to the mooring

line was calculated. This normal component of velocity at each current meter or ADCP bin (bin size 2–5 m) was multiplied by the cross-sectional areas defined by the midpoints between two adjoining moorings or total distance between the mooring and the shore, as appropriate. The outer edge of the mooring line was defined as the same half distance as between the outer mooring and its nearest more coastal neighbor. The vertical boundaries were the surface, the bottom at the mooring site, or the halfway point between instruments/bins as appropriate. The individual mooring transport time series were summed across the section.

3. Results

3.1. Sea Ice

Trajectories from satellite-tracked drifters can provide information on general flow patterns. The trajectories here represent summer and early fall (primarily June–October) flow, when the region is largely ice-free. The

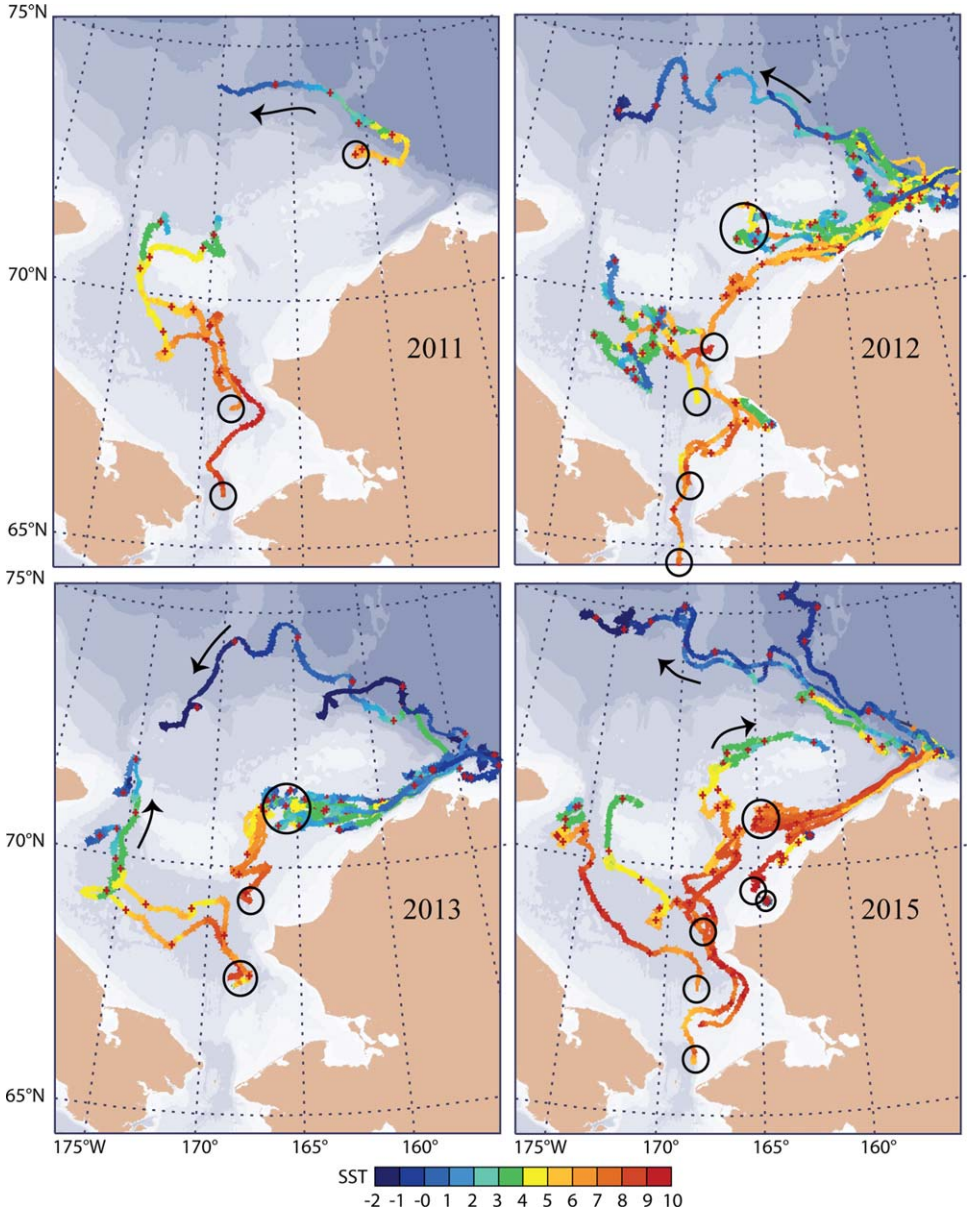

Figure 2. Drifter trajectories (drogue depth 25–30 m) for 4 years. The drifters are color coded by sea surface temperature (scale (°C) is at the bottom). Period between red dots on trajectories is 5 days. For 2011–2013, drifters were deployed in August, while in 2015 drifters were deployed primarily in July. The circles indicate deployment location and the arrows the direction of movement.

4 years in which drifters (drogue depth 25–30 m) were deployed in the Chukchi and northern Bering Sea, trajectories showed the following general flow pattern (Figure 2): northward flow through Bering Strait; a separation south of ~68°N, with some drifters continuing northward into the Central Channel and the remainder transiting westward toward Herald Canyon (see Weingartner et al., 2005; Woodgate et al., 2005b for discussion); a split (~71°N) in Central Channel with most of the drifters moving eastward toward the coast and a few in 2015 continuing northward to circulate clockwise around Hanna Shoal; strong flow northeastward along the Alaskan coast (~71–74°N); and a well-defined northwestward flow along the Chukchi slope from Barrow Canyon toward Herald Canyon (see, in contrast, the eastward flow in the region related to upwelling described by Pickart et al. (2011)). Northward flow through Herald Canyon and anticyclonic flow on the north sides of Hanna and Herald Shoals have been observed by multiple authors (e.g., Brugler et al., 2014; Gong & Pickart, 2015; Weingartner et al., 2013). The paucity of drifters following these latter pathways may be an indication of limited sampling; the drifters were deployed in July and August in ice-free waters and the transit times were such that it was late October by the time they reached Herald Canyon and the two shoals. Autumn brings the arrival of sea ice, which affects the trajectories of the drifters.

While the plots of the drifter trajectories provide an indication of the flow patterns, it is difficult from a casual examination of the plots to determine the average velocity over a large group of drifters. The drifter trajectories do not sample the entire shelf, but in certain regions there are a sufficient number of drifters to obtain an average estimate of velocity. In pursuit of this, we defined eight boxes (Z1–Z8; Figure 3), which contain the trajectories of the vast majority of the drifters, and determined the average trajectory within each box. In each area the length of time it took the drifter to traverse the region and the number of drifters that were used in the estimate is shown. It should be noted that this schematic is derived primarily from data collected during midsummer to midfall.

The flow patterns, shown in Figure 3, are similar to other published maps of the flow pattern (e.g., Figure 1 in Brugler et al. (2014)), with two additions: a well-defined, persistent, eastward flow south of Hanna Shoal toward Icy Cape, and a northwestward flow along the Chukchi slope originating at Barrow Canyon. This latter flow, paralleling the northern Chukchi slope from Barrow Canyon to Herald Canyon, is evident in the trajectories of most of the drifters reaching the slope (Figure 2). Such a west-northwest flow is seen in some years in Shelf Basin Interaction (SBI) mooring data from the region in 2002–2004 (R. Woodgate, T. Weingartner, and K. Aagard, personal communications, 2017).

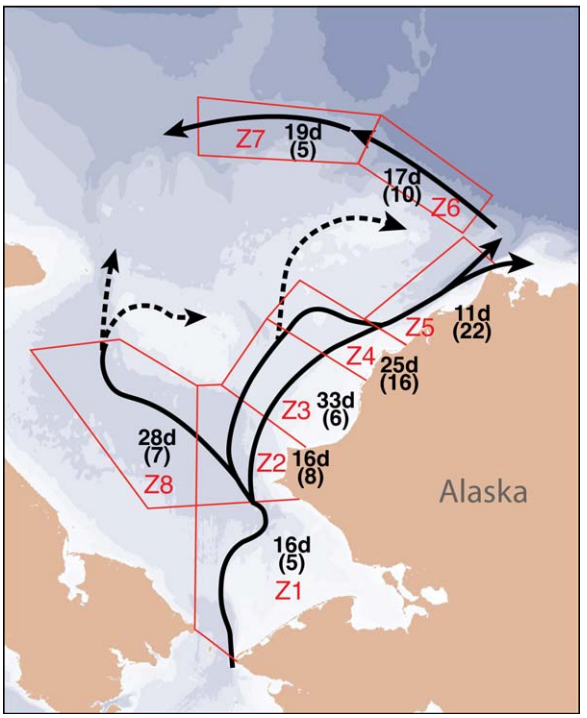

Figure 3. Composite of the drifter trajectories shown in Figure 2. There are eight regions (delineated in red) where the transit times and mean velocities were calculated. The average number of days it took drifters to transit the region and the number of drifters in the estimate (parentheses) are indicated in black. The dashed lines are paths that fewer than two drifters followed.

Most of the other published schematics of flow show a stronger northward flow west of Hanna Shoal that returns southward; this is not evident in the drifter trajectories presented here. The eastward flow (Figure 3) south of Hanna Shoal toward Icy Cape was also evident in flow patterns from ORAS4 operational ocean reanalysis produced by the European Centre for Medium-Range Weather Forecasts (N. Bond, University of Washington, personal communications, 2017). Anticyclonic flow north of Hanna and Herald Shoals appears in the other flow schematics, but is weak in our schematic due, at least in part, to the lack of drifters in the region.

The highest regional mean velocity (~25 cm s^{-1}) was in Barrow Canyon (Z5), with the lowest regional mean velocities being found in regions Z2, Z3, and Z4 (11, 5, and 10 cm s^{-1}, respectively). The remaining zones all had velocities between 15 and 17 cm s^{-1}. These speeds are not dissimilar from measurements obtained from Air-Launched Autonomous Micro Observer (ALAMO) floats (http://www.pmel.noaa.gov/arctic-heat/data), which measured bottom velocities of ~20 cm s^{-1} in zones Z4 and Z5. On average over these summer periods, our results suggest that for a drifter to be advected from Bering Strait to the slope takes ~100 days—approximately the entire summer period during which these measurements were made. Prior work on transit/

residence times of waters in the Chukchi Sea suggest great variability. From a year of measurements of in situ velocity at 11 mooring sites throughout the Chukchi, Woodgate et al. (2005b) indicate transit times of waters through the Chukchi of between 2 and 12 months for the 1990–1991 period, with the time highly dependent both on starting date and starting location. An alternative approach (Woodgate et al., 2010) estimates residence time by comparing the volume of the Chukchi to the volume inflow through Bering Strait. This suggests the residence time has decreased from ~9 months in 2001 to ~5.5 months in 2007 due to the increase in Bering Strait volume transport in this period.

3.2. Currents Measured by Moorings

Since August 2010, moorings have been deployed at selected sites on the northern Chukchi shelf and slope (Figure 1 and Table 1). A total of nine sites had moorings; some for only 1 year and one (C2) for 5 years. The annual mean velocities (Figure 4a) indicate a flow pattern similar to that observed in the drifter trajectories representing just the summer: strong flow in the vicinity of Barrow Canyon (C4 and C5); eastward flow along the Icy Cape transect (C1, C2, and C3); a well-defined Chukchi Slope Current (C9) (Corbett & Pickart, 2017); and weak eastward flow north of Hanna Shoal (C7 and C8) and southeast of Hanna Shoal (C6). Flow measured at the eight sites on the shelf fall into three groups: the Icy Cape line (C1, C2, and C3); the moorings along the coast (C1, C4, and C5); and the three moorings (C6, C7, and C8) nearer Hanna Shoal.

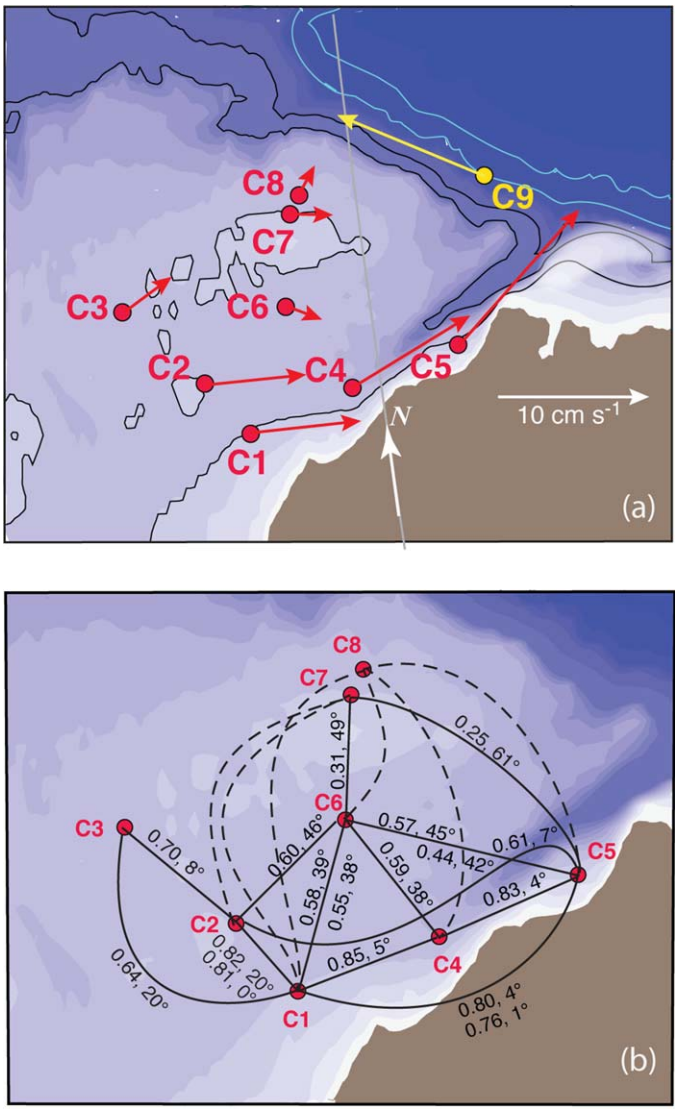

Figure 4. (a) Annual mean bottom velocity at each shelf mooring site (C1–C8) and at 48 m at C9 (b) vector correlations (at a lag of 0 day) among time series of current velocity. The first number is the correlation of vectors and the second number is the rotation angle between the two vector time series. Dashed lines indicate no significant correlation ($p > 0.05$), black lines indicate that correlations are significant at $p < 0.01$ except for C7 to C5 for which $p = 0.05$. Multiple correlations for some pairs (e.g., C1 and C2) represent separate correlations for different years. The shelf flow is not correlated with that at C9 ($p > 0.5$).

3.2.1. Time Series of Near-Bottom Currents at Icy Cape (C1, C2, C3)

The first three moorings (C1, C2, and C3) stretch in a line across the shelf starting at Icy Cape and extending ~180 km offshore in a northwest direction (Figure 1). This line was approximately normal to the coastline. September hydrographic surveys show the water column is two-layered with cold, saline bottom water overlain by warmer, fresher waters (Figure 5), a structure typical of the eastern Chukchi (e.g., Coachman et al., 1975; Woodgate et al., 2015). The innermost mooring (C1) was deployed in Alaskan Coastal Water, evident by the low salinity and warmer water in the upper layer (Coachman et al., 1975; Danielson et al., 2017; Gong & Pickart, 2015; Paquette & Bourke, 1974; Woodgate & Aagaard, 2005). The other two moorings were deployed farther off the coast in what likely originated as Bering Shelf Water (Coachman et al., 1975).

The mean near-bottom currents were largely eastward (Figure 4a) with the strongest flow (7.3 ± 0.9 [mean $\pm$ standard error of the mean] cm s^{-1}; 4 year average) found at C1 and the currents decreasing with distance from the coast (5.3 ± 0.5 cm s^{-1}; 5 year average at C2 and 3.9 ± 0.6 cm s^{-1}; 2 year average at C3). Looking at seasonal means, the strongest flow was in the spring/summer (Table 2), but the strongest daily averaged currents were found in the fall and winter when the system was largely ice covered (Figure 6). This is very similar to the flow conditions observed in Bering Strait (e.g., Woodgate et al., 2005a). Horizontally, the low-pass filtered currents at Icy Cape are in phase and well correlated ($p \ll 0.001$, Figure 4b).

During the cold season (November–April), strong reversals (flow toward the south-southwest) were common (Figure 6). At C1, these periods of southwestward flow were often associated with inflow of relatively warm (>1°C) Atlantic Water (Ladd et al., 2016), and as observed by prior work (e.g., Aagaard & Roach, 1990; Bourke & Paquette, 1976; Garrison & Becker, 1976; Mountain et al., 1976; Woodgate et al., 2005b). Ladd et al. (2016) also noted that the number of

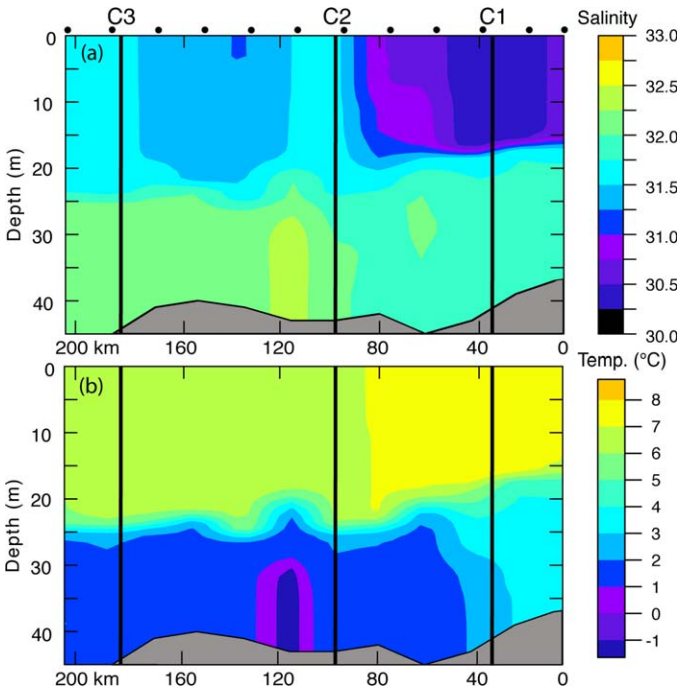

Figure 5. Cross sections at Icy Cape for (a) salinity (practical salinity units) and (b) temperature (looking north). Locations of the C1, C2, and C3 are indicated. Data were collected in 25–26 August 2011. Note that C1 is in the low-salinity core of the ACC. The dots indicate locations of CTD casts.

occurrences of Atlantic Water varied seasonally (usually occurring between October and May) and among years with 2010–2011 having more events (3) than the other years. These periods of Atlantic water were often associated with polynyas, as discussed in Ladd et al. (2016).

3.2.2. Time Series of Bottom Currents Along the Coast (C1, C4, C5)

The strongest shelf flows occurred at the three mooring sites (C1, C4, and C5) nearest the coast, with strongest (12.1 ± cm s^{-1}; 2 year average) mean flow occurring at C5, slightly weaker (9.1 ± 3.0 cm s^{-1}; 1 year average) flow at C4 and the weakest (7.3 ± 0.9 cm s^{-1}; 4 year average) at C1 (Figure 4a). The mooring site C5 was on the east side of Barrow Canyon and C4 was near the head of the canyon. The magnitude of the daily average velocity varied similarly at the three sites (Figure 7), with the maximum magnitude decreasing from C5 (∼100 cm s^{-1} in January) to C4 (∼80 cm s^{-1} in December), to C1 (∼60 cm s^{-1} in December). Ladd et al. (2016) observed that the propagation of the identifiable Atlantic Water events observed at C1, C4, and C5 indicated that C5 lead C4 by ∼1 day and C1 by ∼4 days, suggesting that the source of Atlantic Water was upwelling via Barrow Canyon. The time series at the mooring sites are well correlated ($p \ll 0.001$; Figure 4) with C5 leading C1 by ∼6 h, although lag is not significantly different from 0 h.

Similar to the time series at Icy Cape, the mean seasonal velocities at C4 and C5 during spring/summer were more than twice those during the fall/winter, and the standard deviations much weaker (Table 2). Once again, the greatest variability in daily flow occurs in fall through early spring, with currents in midspring through summer more steady in both direction and speed.

3.2.3. Time Series of Bottom Currents East and North of Hanna Shoal (C6, C7, C8)

The last three moorings sites on the Chukchi shelf (C6, C7, and C8) had the weakest mean flow (Figure 4) with averages of 2.4 cm s^{-1} (2 year average) at C6, 2.8 cm s^{-1} (1 year average) at C7, and 2.1 cm s^{-1} (1 year average) at C8. In addition, these moorings had the weakest maximum daily average currents (Figure 8). While the average flow was eastward at each of the mooring sites, reversals were common. The single year of current data at C8 was not significantly ($p = 0.05$) correlated with the currents at any of the other mooring sites (Figure 4b), while the currents at C7 were weakly correlated with C5 ($p = 0.05$) and better correlated with those at C6 ($p = 0.01$).

Like the other shelf moorings, the mean near-bottom currents at C6 and C7 were the strongest during the spring/summer period (Table 2). In contrast to the other sites, however, the mean bottom currents during winter at C8 were >60% stronger than those during the spring/summer.

3.3. Correlations: Currents and Winds

The time series were divided into two seasons: "winter" (1 November to 31 March) when the region was largely ice covered and "summer" (1 May to 30 September) when there was little or no ice in the vicinity of the moorings. As noted before, except for C8, the mean velocity in winter is weaker than that of summer. Interestingly, the near-bottom average currents were generally stronger than the flow in the water column (see Table 2, bold). This is especially true in winter when, of the 15 time series, only at C5 (2013–2014) were the currents in the middle of water column stronger than those at the bottom. In contrast, during summer for only 8 of the 15 time series was the bottom net velocity the strongest, with weaker net bottom velocities occurring primarily at C1 and C5, two of the more coastal moorings. Even with these differences in magnitude, at each of the eight shelf sites, the currents were highly correlated ($p \ll 0.001$) in the vertical (Table 2).

The bottom currents measured at sites C1–C6 were all significantly correlated with the NARR winds ($0.4 < r < 0.6$, $p \ll 0.001$) with the winds leading the currents by 12–18 h. These were vector correlations and the currents were generally 10–30° to the right of the winds. Interestingly, the bottom currents at C7 and C8

Table 2
The Depth, Net Velocity (NV) ± RMS, and Net Direction (α) Together With the Vertical Correlations Between the Selected ADCP Bins and the Bottom Most Bin (Bot. Depth)

		Winter (1 Nov to 31 Mar)			Summer (1 May to end of record)		
	Year	Bot. depth NV ± RMS α	Depth (m) and net vel ± RMS theta	Corr. (R, β)	Bot. depth NV ± RMS α	Depth (m) and net vel ± RMS theta	Corr. (R, β)
C1	2010–2011	33 m **8.0** ± 3.9 67°	5 m 2.7 ± 3.6 54°	0.91 −6°	33 m 11.0 ± 1.9 73°	5 m 1.8 ± 2.7 315°	0.53 −8°
			19 m 7.8 ± 4.1 66°	0.98 −7°		19 m 11.0 ± 2.5 76°	0.98 −4°
	2013–2014	35 m **5.5** ± 4.4 123°	11 m 3.9 ± 3.8 155°	0.95 −6°	35 m 12.0 ± 3.4 101°	11 m 9.3 ± 4.3 98°	0.93 −16°
			19 m 4.2 ± 4.4 137°	0.97 −7°		19 m 12.2 ± 4.0 99°	0.96 −12°
	2014–2015	30 m **3.8** ± 3.2 87°	6 m 0.3 ± 3.6 300°	0.95 −4°	30 m 12.8 ± 2.8 72°	6 m 11.5 ± 2.8 66°	0.92 −14°
			14 m 2.0 ± 3.8 59°	0.97 −4°		14 m 13.1 ± 2.8 72°	0.95 −10°
C2	2010–2011	31 m **6.8** ± 2.4 78°	7 m 5.7 ± 2.9 72°	0.92 −7°	31 m 8.2 ± 1.6 104°	7 m 6.6 ± 2.3 89°	0.87 −6°
			15 m 6.7 ± 2.7 75°	0.96 −7°		15 m 8.1 ± 1.9 98°	0.93 −7°
	2011–2012	32 m **4.4** ± 1.7 96°	4 m 2.6 ± 1.9 116°	0.90 −1°	32 m **9.6** ± 1.9 98°	4 m 7.8 ± 3.0 102°	0.81 −18°
			16 m 4.2 ± 1.7 99°	0.98 −1°		16 m 9.3 ± 1.9 102°	0.94 −14°
	2013–2014	35 m **3.5** ± 2.6 81°	5 m 1.6 ± 2.2 174°	0.86 −4°	37 m 8.9 ± 1.6 107°	5 m 5.5 ± 2.5 112°	0.75 −19°
			15 m 2.2 ± 2.9 85°	0.94 −8°		15 m 8.9 ± 2.0 108°	0.88 −9°
C3	2010–2011	32 m **5.0** ± 1.7 84°	6 m 3.3 ± 1.9 79°	0.87 −2°	32 m **7.3** ± 1.4 72°	6 m 5.9 ± 2.1 36°	0.72 −3°
			16 m 4.8 ± 1.8 81°	0.95 −4°		16 m 7.1 ± 1.8 63°	0.88 −5°
	2011–2012	33 m **3.7** ± 1.1 39°	5 m 0.5 ± 1.2 6°	0.83 −6°	33 m **6.7** ± 1.1 52°	5 m 4.4 ± 2.1 38°	0.68 −11°
			15 m 3.2 ± 1.2 32°	0.97 1°		15 m 6.4 ± 1.2 50°	0.87 −5°
C4	2014–2015	34 m **5.4** ± 4.2 67°	6 m 4.4 ± 2.8 358°	0.96 −8°	34 m **18.7** ± 2.5 71°	6 m 15.5 ± 2.5 71°	0.89 −16°
			18 m 4.4 ± 4.1 44°	0.98 −6°		18 m 17.8 ± 2.4 77°	0.96 −15°
C5	2013–2014	33 m 10.3 ± 4.6 355°	5 m 10.8 ± 5.5 346°	0.90 −12°	33 m 21.3 ± 4.7 56°	5 m 20.0 ± 10.3 271°	0.75 −16°
			17 m 10.7 ± 4.1 2°	0.96 −10°		17 m 24.0 ± 5.9 61°	0.89 −8°
	2014–2015	35 m **5.0** ± 4.5 56°	9 m 3.5 ± 6.0 310°	0.95 −12°	35 m 20.1 ± 2.9 67°	9 m 22.8 ± 3.5 73°	0.94 −16°
			17 m 1.8 ± 4.6 2°	0.97 −10°		17 m 23.2 ± 3.4 75°	0.96 −12°
C6	2013–2014	30 m **2.4** ± 1.7 107°	8 m 0.8 ± 2.1 265°	0.68 25°	30 m **3.6** ± 1.3 148°	8 m 2.1 ± 1.6 165°	0.79 −7°
			14 m 0.9 ± 12.0 52°	0.91 −2°		14 m 2.7 ± 1.6 156°	0.85 −3°
	2014–2015	30 m **2.5** ± 1.4 88°	6 m 3.3 ± 1.5 261°	0.85 15°	30 m **3.4** ± 1.4 127°	6 m 4.8 ± 2.4 217°	0.56 −8°
			14 m 1.8 ± 1.5 22°	0.97 1°		14 m 3.3 ± 1.6 124°	0.88 −9°
C7	2013–2014	32 m **2.1** ± 1.0 51°	4 m 2.1 ± 1.9 303°	0.64 −3°	32 m **5.2** ± 1.5 110°	6 m 3.7 ± 2.1 101°	0.72 −4°
			14 m 2.0 ± 1.0 0°	0.81 −3°		14 m 5.1 ± 2.0 106°	0.84 −5°
C8	2014–2015	30 m **3.7** ± 0.8 10°	6 m 1.7 ± 1.2 294°	0.74 8°	30 m **2.2** ± 1.8 82°	6 m 0.5 ± 1.9 91°	0.80 8°
			14 m 2.9 ± 0.9 344°	0.87 2°		14 m 1.3 ± 2.4 70°	0.88 3°

Note. The vector correlations (R) are given for each year an ADCP functioned. These are vector (complex) correlations, so the angle (β) is also indicated. Note that the bottom leads top for negative lag. All correlations are at 0 lag, since maximum correlations are not significantly different. For all correlations $p < 0.001$. Bold indicates when bottom velocity is largest.

were not significantly ($p > 0.01$) correlated with the winds. This coincides with the weak correlations of currents at C7 and C8 with those at C1–C6 (Figure 4b). These results are consistent with earlier findings of high correlations between wind and currents in some, but not all regions of the Chukchi. Using a 1 year 11 mooring array throughout the Chukchi, Woodgate et al. (2005b) found correlations between model surface winds and measured water velocities of ~0.75 in the Bering Strait region; 0.5–0.6 in the central Chukchi (highest values near the Alaskan coast); and 0.6 on the north side of Long Strait and in Barrow Canyon. However, along the Russian coast and in Herald Valley, correlations between wind and water velocity were 0.25 or less.

3.4. Chukchi Slope Current

The drifters exiting Barrow Canyon usually turned sharply westward and followed the shelf break (Figure 2). On exiting the shelf, there was a marked change in the sea surface temperature measured by the satellite-tracked drifters, especially evident in 2015. This is a result of the water on the shelf being denser than the near-surface water at the slope, as evident in Figure 9. As it flows down Barrow Canyon, the warmer (>7°C), denser (>24.0) shelf water sinks below the colder, lighter, surface slope water. Although the satellite-

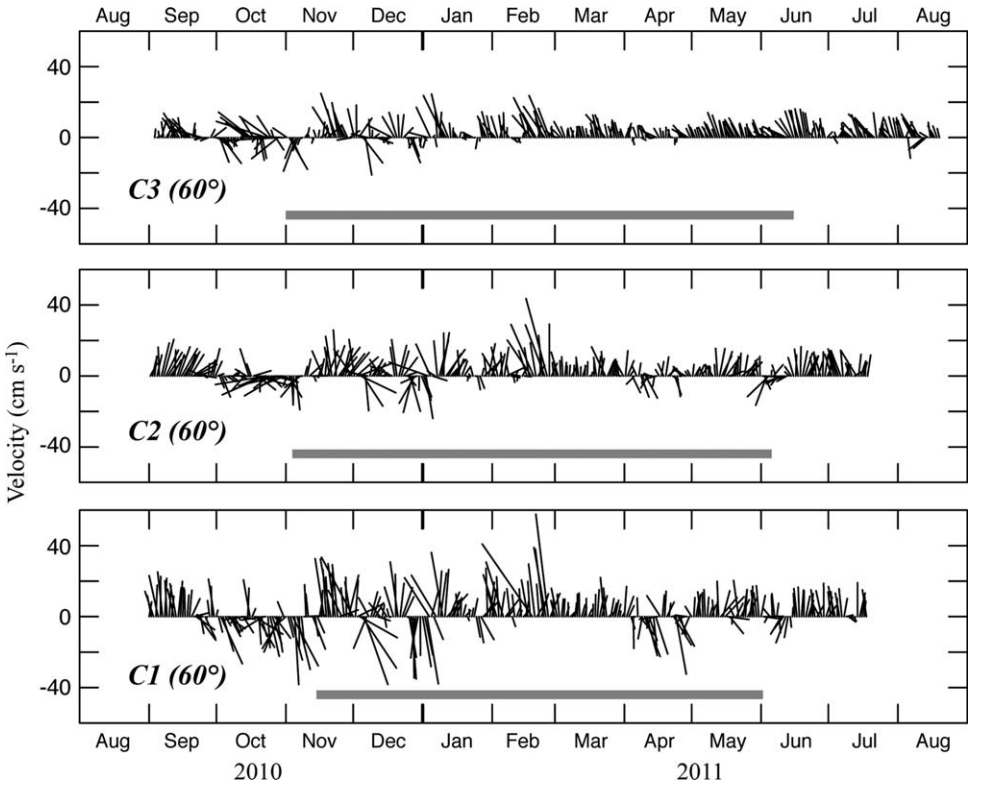

Figure 6. Low-pass filtered bottom velocity (daily) data from C3, C2, and C1. The rotation of the velocity axes is indicated in parentheses so upward is approximately northeastward. The shaded line at the bottom is when ice is present (>40% areal coverage), using AMSR-E data set.

tracked drifters were drogued at 25–30 m, the thermistor was at the surface; so as the shelf water sinks, the temperature at the surface appears to cool. How much of the shelf water turns westward and follows the slope and how much turns eastward or continues northward to enter the basin is unclear and likely time-dependent, but from the drifter trajectories two things are evident. First, none of the drifters, continued northward into the basin. Second, of the 18 drifters that exited Barrow Canyon, 12 turned westward moving along the slope, four turned eastward (usually before reaching the slope) and two were "undecided," failing to take either route before sea ice arrived to limit the drifters' movement.

The mooring at C9 measured the currents on the ~950 m isobath (Figure 10). The flow was strongest in the "warm" months (June–October) when ice cover was limited and weakest in January–March when the region was ice covered. Evidence of this seasonal cycle can be seen to at least a depth of ~300 m (Figure 11). Flow at 900 m was extremely weak (Figure 10) and not statistically different from 0 cm s^{-1}.

At C9, the only instrument measuring both temperature and salinity was at ~300 m. The average annual potential temperature was 0.71°C (standard deviation of 0.04°C) and the average annual salinity of 34.77 (standard deviation of 0.01), which is identified as Atlantic Water (Corbett & Pickart, 2017). Only temperature was measured at 900 m and the average potential temperature was ~0.0°C (standard deviation of 0.03°C), which is typical of Arctic deep water in the Canada Basin.

3.5. Icy Cape

3.5.1. Transport

Transport was calculated at the Icy Cape line for 2010–2011 following Stabeno et al. (1995, 2016) and Stabeno and Hristova (2014) and as described in section 2. During this 1 year long deployment all three ADCPs functioned. The question arises on how good the estimate of transport is for 2010–2011. Sources of error in the transport estimate for 2010–2011 include velocities that are unresolved in the vertical or between the moorings, and uncertainties in the horizontal extent of the currents represented by the mooring line. The high vertical correlations (Table 2) and the flatness of the bottom give confidence to the vertical

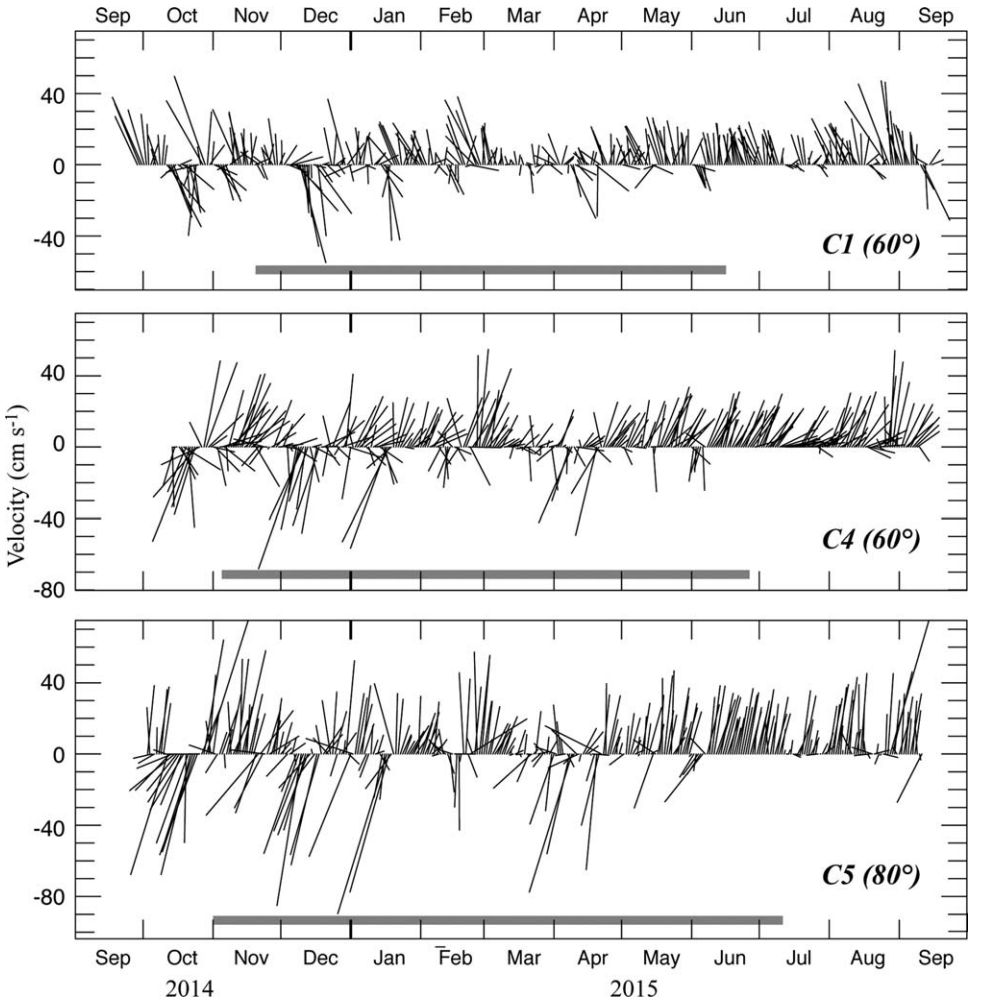

Figure 7. Low-pass filtered bottom velocity (daily) data from C1, C4, and C5. The rotation of the velocity axes is indicated in parentheses so that upward for top two time series is approximately northeastward and for the bottom time series is approximately eastward. The shaded line at the bottom is when ice is present (>40% areal coverage).

extrapolation to the surface and the ocean bottom. Significant correlations between the three moorings (Figure 4) also lend support to reliable interpolation between moorings. The largest source of uncertainty is in the horizontal extent of the transport estimate (i.e., the area shoreward of C1 and seaward of C3). Site C1 is ~50 km seaward of the 5 m isobath and ~30 km seaward of the 40 m isobath and is within the coastally intensified current that extends ~70 km from the coast (Fang et al., 2017). The transport estimate included the areal extent to the 40 m isobath, so the inner 20 km, which shoals from 40 to 5 m was not included in the transport calculation. If the currents at C1 continued inshore to the coast, the calculated transport would be an underestimate of ~0.02 Sv, or 5% of total transport. However, Fang et al. (2017) show considerable variability in surface flow in the near-shore region and so this is only a rough estimate. The extent of the current offshore of measurements at C3 is a more difficult question. Our estimates used 45 km (half the distance to C2). This seemed a reasonable estimate considering the slight decline in speed between C2 (~5.3 cm s^{-1}) and C3 (3.9 cm s^{-1}). If instead of 45 km, we used only 22.5 km, the total transport would be reduced by 0.04 Sv, or ~10%. The above error estimates (underestimating inshore and overestimating offshore) suggest that our calculations of transport are probably good to ±10%.

In none of the following years were there ADCP data from each of the three mooring sites. Thus, an estimate of transport for each later year was made by regressing the 2010–2011 transports (calculated using all three ADCP records) on the subset of data available for a given deployment. For example, in 2011–2012, the ADCP data at C2 and C3 and the bottom currents (RCM9) at C1 were available. Selecting analogous data

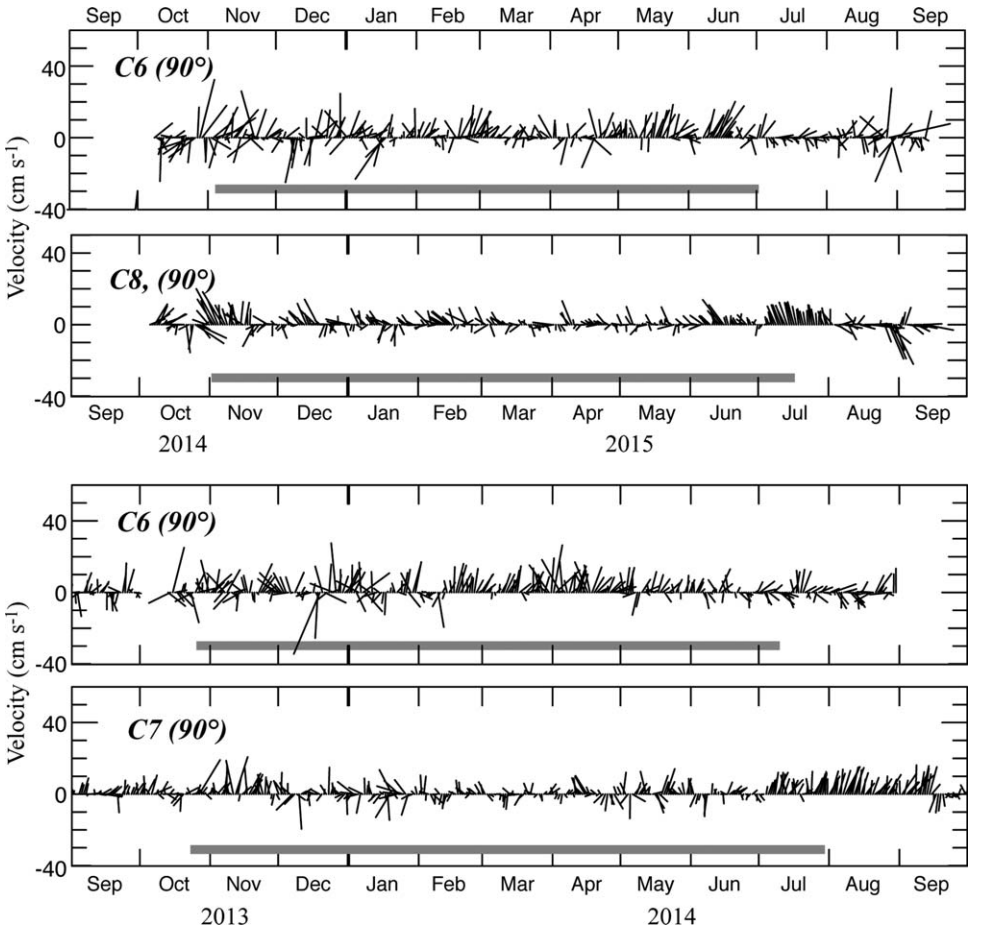

Figure 8. Low-pass filtered bottom velocity (daily) data from C6, C7, and C8. The vectors were rotated 90° (upward is eastward). The shaded line at the bottom is when ice is present (>40% areal coverage).

from 2010 to 2011 data set, the best fit regression formula was calculated (Table 3) and the correlation (R^2) between the 2010 and 2011 transport and the estimated transport using the regression formula was calculated. It is not surprising that the weakest correlations were for 2012–2013 when only the bottom velocity at C2 was measured, but even then 87% of the variance was accounted for. Using these linear regressions and the time series of currents collected each year (2011–2015), estimates of transport were calculated (Figure 12).

The time series are dominated by short-term (several days) variability. The strongest variability was generally in fall through early spring, with the daily transports ranging from approximately −6 Sv (southwestward flow) to 5 Sv (northeastward). The average transports for each deployment varied from 0.24 Sv in 2011–2012 to 0.55 Sv in 2014–1015 (Table 3). For each year, the transport at Icy Cape ranged from ∼30% to ∼45% of the transport through Bering Strait. The average transport over the 5 years of data was 0.40 Sv or ∼40% of the transport through Bering Strait during that time period.

The transports were significantly ($p \ll 0.01$) correlated with the local winds (Table 3), but annually the correlations varied significantly among years. The weakest correlation ($R^2 = 0.21$) was in 2012–2013 and the strongest was almost twice that ($R^2 = 0.39$) in 2014–2015. These relationships did not vary with which time series were used to calculate transport. For instance, 2010–2011 (calculated using ADCP data from C1, C2, C3) and 2012–2013 (calculated using data from only C2) had similar R^2. Correlation between wind and transport vary seasonally. Correlations are weaker ($R^2 = 0.25$, $p \ll 0.01$) during winter than during summer ($R^2 = 0.33$, $p \ll 0.01$). This may be the result of the presence of ice. As suggested by Martin et al. (2014), wind stress is transferred less effectively through pack ice than open water.

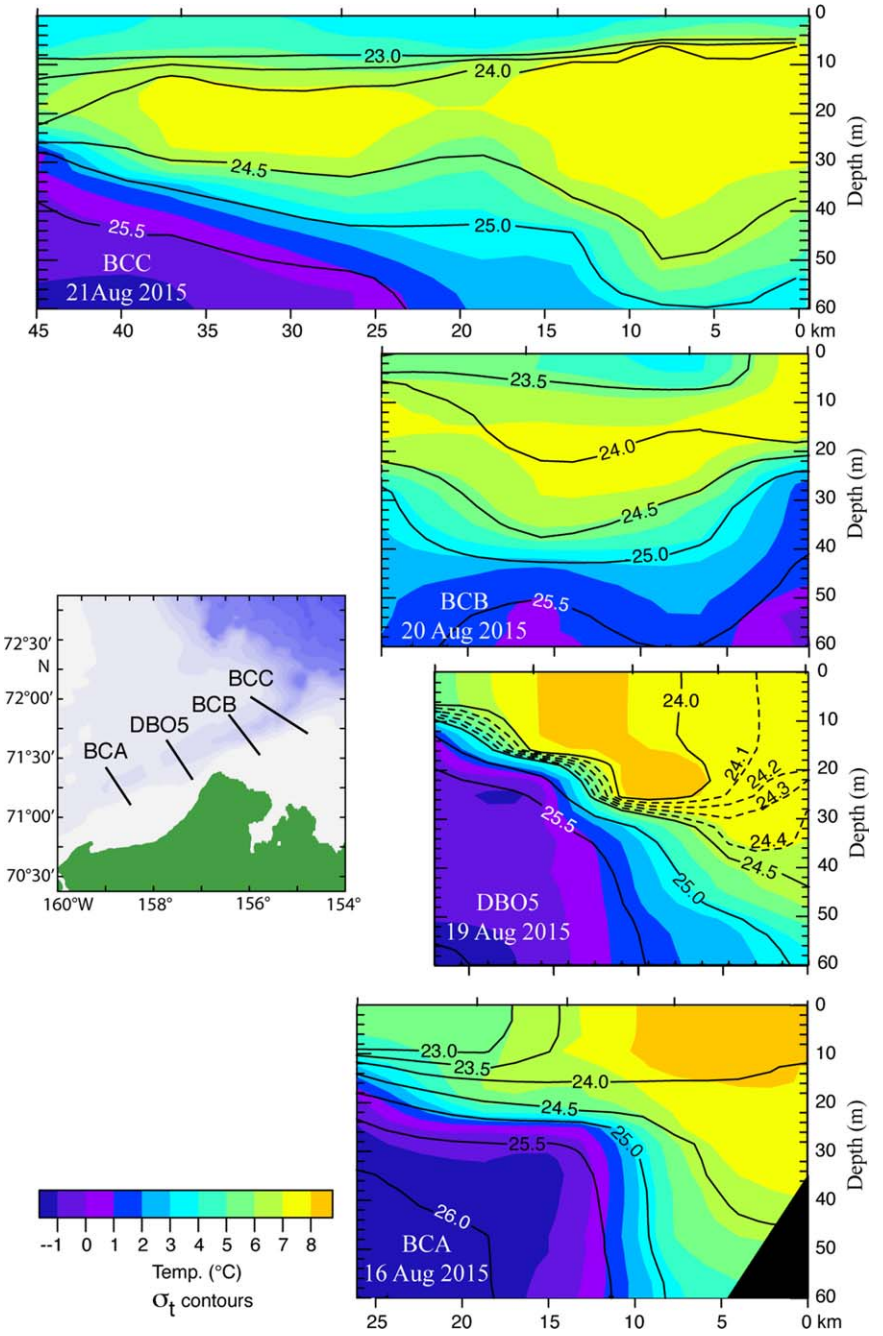

Figure 9. Cross section of temperature (colored) and density (contours) at four transects covering Barrow Canyon (box in Figure 1). Locations of the transects from south (bottom) to north (top) are shown in the map at the left. Tick marks at the top of plots indicate station locations.

A wind-rose (Figure 13b) shows that the dominant direction of the wind is toward the southwest quadrant (180–270°). The magnitude of transports was clearly dependent upon wind direction (Figure 13c). Only when the winds were toward −180 to −120° was the average transport at Icy Cape southwestward. The strongest transports were toward the northeast and occurred when the winds were toward −30–60°.

The current records at C1, C2, and C3 during 2010–2011 were divided into groups according to wind direction (Figure 14). During times when the wind speed was greater than 2 m s^{-1} and toward the southwest (150–240°), the flow was southwestward except the near-bottom flow at C3. The strongest currents were >10 cm s^{-1} toward the southwest in the near-surface at C1. In general, the southwestward velocity

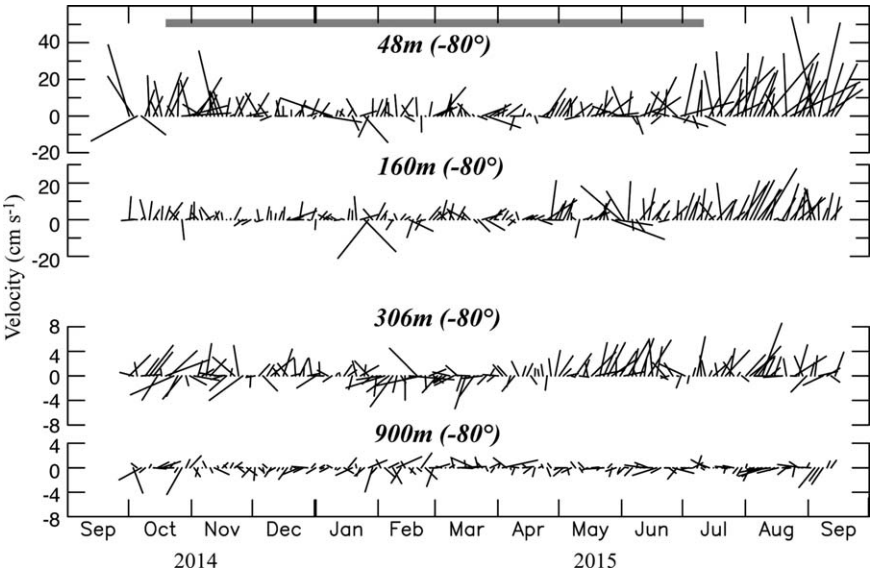

Figure 10. Low-pass filtered velocity (daily) data from selected depths at C9. The vectors were rotated −80° (upward is approximately westward). Note the bottom two time series have different scales from the top two time series. The shaded line at the top is when ice is present (>40% areal coverage).

decreased with depth. This provides an explanation of why maximum mean flows were typically at the bottom (Table 2). In sharp contrast, when the winds were toward the northeast (−30–60°), the currents were also strongly northeastward, with the strongest flow near the surface and weakening with depth.

3.5.2. Near-Bottom Temperature and Salinity

Ocean temperature and salinity varied strongly on multiple time scales at the bottom at C2 (Figure 12). The water column was primarily well mixed during winter and two-layered during summer. When the water column was covered with ice, bottom temperatures were close to the freezing point for most of the winter except during intrusions of warmer Atlantic Water (Ladd et al., 2016). At times (dots below the axis in Figure 12), a sharp increase in salinity is associated with slight cooling that may be a result of brine rejection from freezing. Other increases in salinity, however, have no corresponding change in temperature. From late fall through midspring, salinity was highly variable. The causes of variability are not always evident—sometimes southwestward transport was associated with increased salinity, but other times it was not. This variability is indicative of the spatial complexity of water masses on this shelf.

The bottom temperatures were much more variable during summer as the retreat of ice allowed interaction with atmosphere, including the occurrence of episodic mixing events, and the advection of pools of warmer

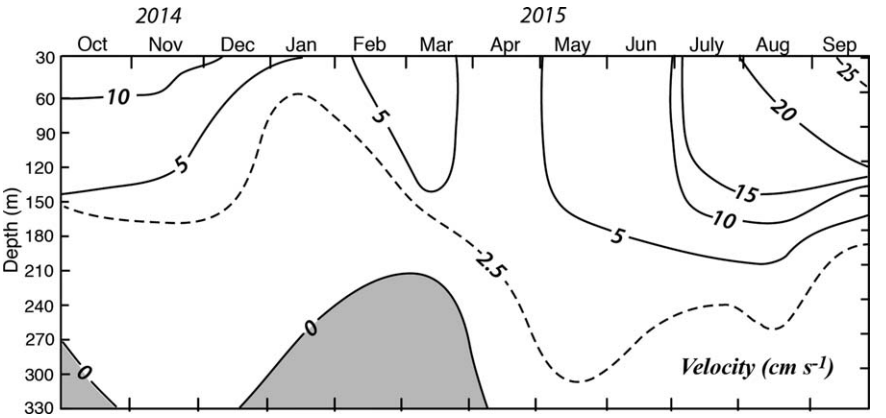

Figure 11. Contours of low-pass filtered currents (−80°) from the ADCP at C9. Positive is approximately westward flow. The shaded areas represent negative (approximately eastward) flow.

Table 3
Statistical Analysis for Calculation of Transport at Icy Cape

Start and end time	Instruments	Regression formula	Cor. R^2	Mean ± SE (Sv)	Min/Max (Sv)	Wind Cor. R^2
3 Sep 2010 to 20 Aug 2011	ADCP—C1, C2, C3	$(D_1{*}V_1 + D_2{*}V_2 + D_3{*}V_3) \times 10^{-6}$	1.00	0.45 ± 0.08	−2.73/4.98	0.22
29 Aug 2011 to 19 Aug 2012	ADCP—C2, C3 RCM9—C1	$(0.037{*}B_1 - 0.031) + (D_2{*}V_2 + D_3\,V_3) \times 10^{-6}$	0.99	0.24 ± 0.08	−4.53/3.67	0.28
26 Aug 2012 to 24 Aug 2013	RCM9—C2	$0.111{*}B_2 - 0.019$	0.83	0.46 ± 0.08	−3.55/3.10	0.21
30 Aug 2013 to 22 Sep 2014	ADCP—C1, C2	$(D_1\,V_1 + D_2\,V_2) \times 10^{-6} + 0.014\,{*}(U_1 + U_2)/2 + 0.049$	0.97	0.33 ± 0.07	−5.79/3.26	0.025
28 Sep 2014 to 10 Sep 2015	ADCP—C1 RCM9—C2	$D_1{*}V_1 \times 10^{-6} + 0.051{*}B_2 + 0.049$	0.96	0.55 ± 0.17	−5.05/5.01	0.39
		Average		0.39 ± 0.03	−5.79/5.01	0.25

Note. Where $D_1 = 89 \times 10^3$ m, $D_2 = 73 \times 10^3$ m, and $D_3 = 90 \times 10^3$ m are the distances around moorings. B_1 is the bottom velocity (cm s^{-1}) from the RCM at C_1, and similarly for B_2 and B_3. U_1 is vertically averaged velocity (m s^{-1}) at C_1, and similarly for U_2 and U_3, and V_i = depth of water column × U_i, for i = 1, 2, 3. SE (the standard error of the mean) = S/N^5, where N is the number of independent estimates. The last column is the correlation between the transport and the local winds.

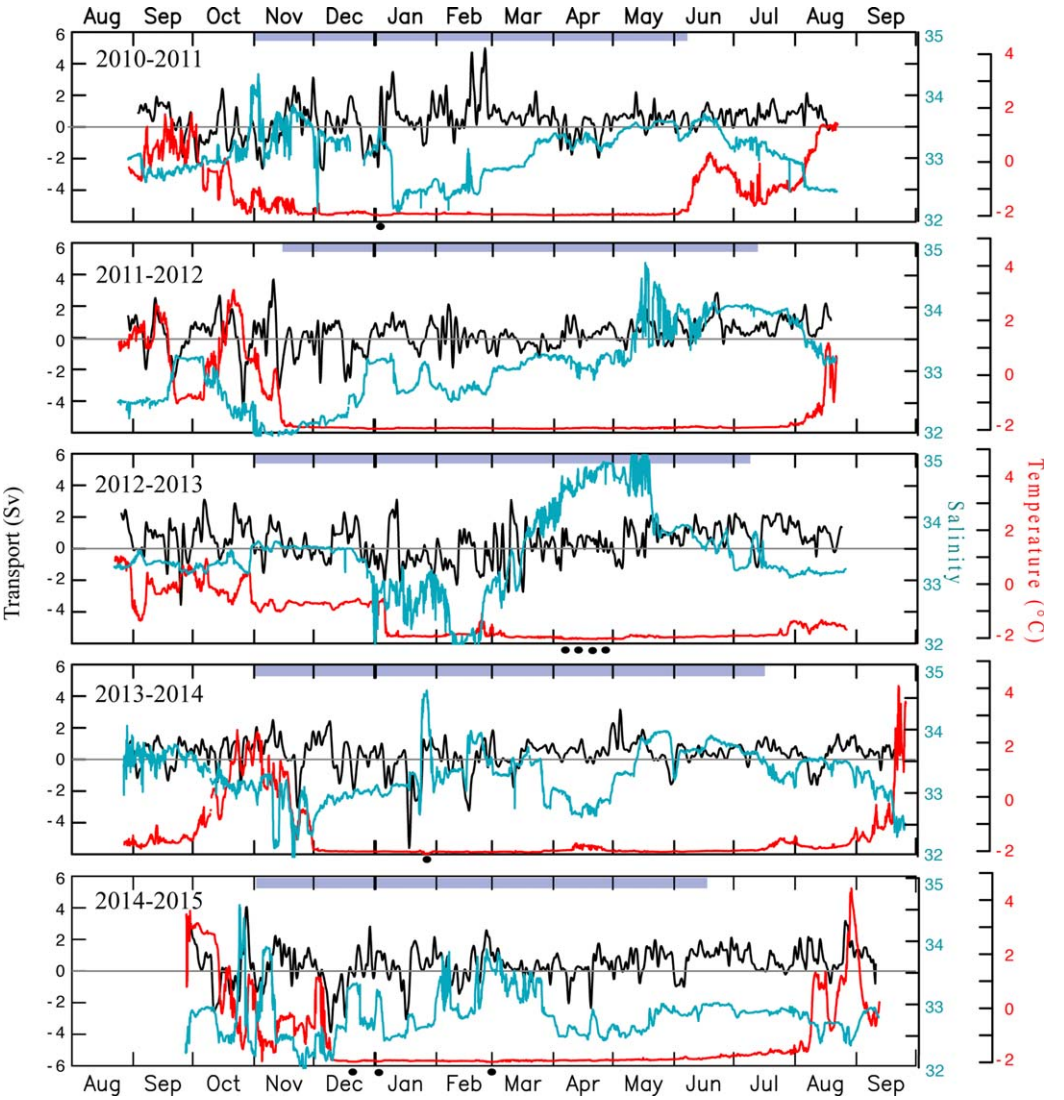

Figure 12. Time series (low-pass filtered) of total transport (black) calculated on the Icy Cape section using time series of currents perpendicular to the mooring line (i.e., toward the northeast [45°]). The bottom temperature (red) and the salinity (blue) measured at C2. The dots indicate times of increasing salinity and cold temperatures.

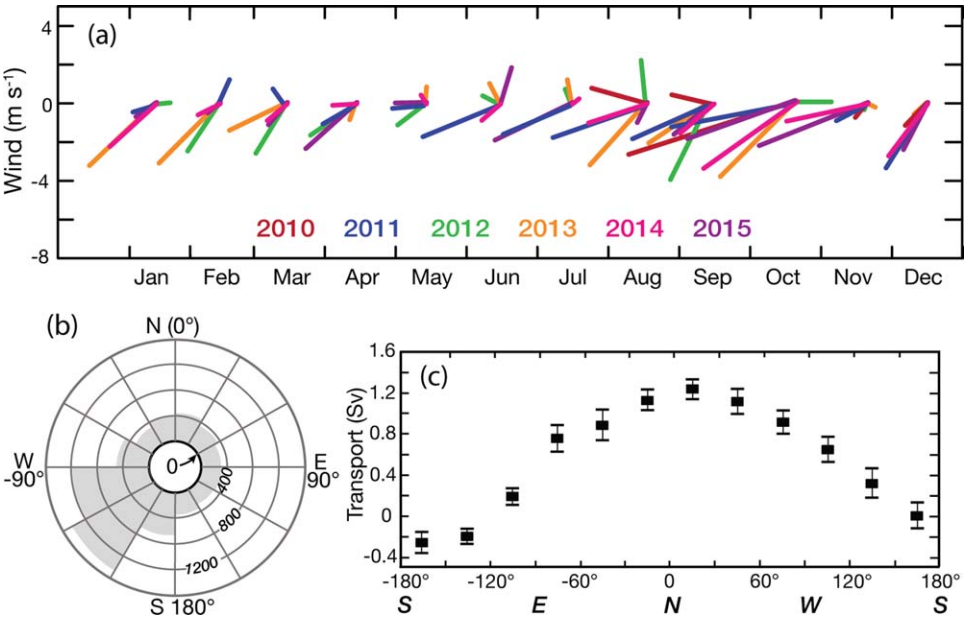

Figure 13. (a) The monthly mean wind velocity vectors for September 2010 to September 2015 color coded by year. (b) A histogram of 6 hourly wind direction (winds toward that direction) (speed > 2 m s^{-1}) for the same period as in Figure 13a. (c) The mean transport for each 30° band of wind direction shown in Figure 13b. The error bars are the standard error of the mean.

Bering Shelf Water past the mooring sites. Episodic mixing events are especially evident during late summer and early fall, when the bottom water freshens and warms as the fall storms mix the warmer, fresher surface waters downward.

3.5.3. Monthly Transport at Icy Cape and Its Relationship to Bering Strait

There is strong seasonal variability in the monthly mean transport at Icy Cape, both in individual years and when averaged over the deployment period (September 2010 to September 2015) (Figure 15). The monthly mean transports during winter and fall were highly variable, but transport was northeastward with less variability in April–July. Comparing the average (September 2011 to July 2015) monthly transports at Icy Cape with those through Bering Strait shows a similarity in the temporal pattern (red and blue lines). Both have the strongest flow in late spring and summer and the weakest in the late fall and early winter. There is also

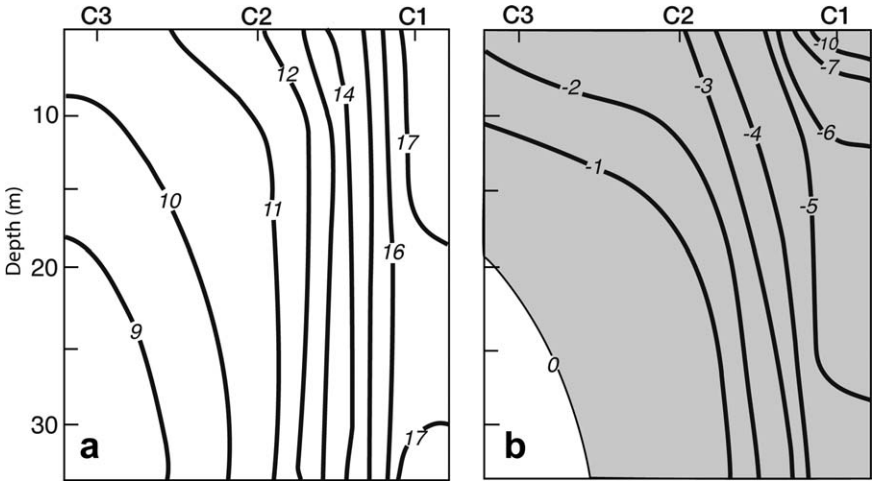

Figure 14. Contours of mean flow perpendicular to the Icy Cape mooring line when (a) winds (>2 m s^{-1}) are toward the northeast (-30–60°) and (b) when winds (>2 m s^{-1}) are toward the southwest (150–240°). Positive is flow toward the northeast and negative (shaded) is flow toward the southwest.

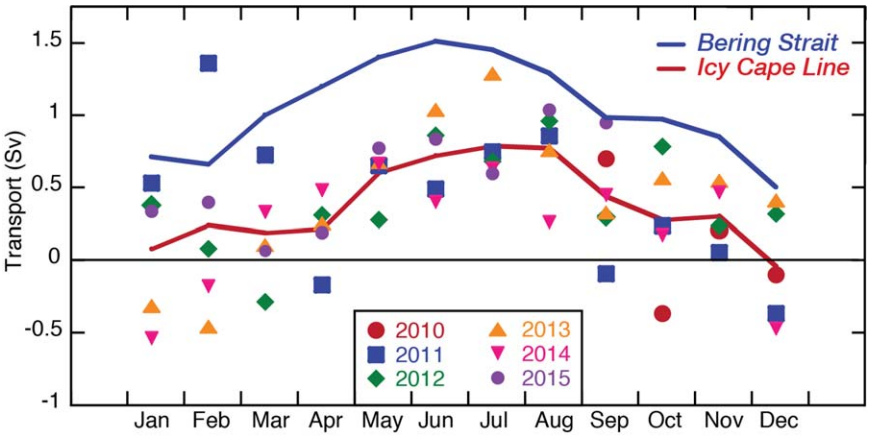

Figure 15. Total transport calculated at the Icy Cape transect using mooring data. The red line is the average transport calculated at Icy Cape and the blue line is the average monthly transport through Bering Strait for the same years. The colors for each year are the same as in Figure 13a.

a seasonal pattern in ratios of the transport at Icy Cape and that at Bering Strait, with the largest ratios (0.44–0.57) occurring in June–September and the smallest (<0.2 except for February, which was 0.35) occurring in December–April. The ratios during individual summer months can be larger, for instance reaching 0.86 in July 2013.

The monthly mean transports between Icy Cape and Bering Strait (September 2011 to July 2015) are significantly correlated ($R^2 = 0.35$, $p \ll 0.01$) likely, because of the strong seasonal signal in transports that occurs at both locations. This is not unexpected, since local transports are correlated with winds and the winds at the two sites are also well correlated ($R^2 = 0.54$, $p \ll 0.01$). The correlation between the monthly anomalies from the seasonal signals, however, is also significant ($R^2 = 0.15$, $p = 0.01$), albeit much weaker.

4. Discussion and Summary

The 5 years of data collected as part of three BOEM programs provide insight into the flow patterns on the northern Chukchi shelf. The flow is strongly influenced by bathymetry. The flow patterns on the shelf are fairly well known, and results from this study (current measurements and satellite-tracked drifter trajectories) contribute to the refinement of earlier maps of currents. The flows in the vicinity of Barrow Canyon are comparable to prior annual means (e.g., 14.4 ± 3.2 cm s^{-1}; 1990–1991, Woodgate et al., 2005b). The major modifications to previous understanding of the flow patterns include: the strong eastward flow south of Hanna Shoal, the weak flow to the north, and the presence of the Chukchi Slope Current (Figure 16).

Data from C9 are the first mooring data measuring the Chukchi Slope Current (Corbett & Pickart, 2017). The current meter data together with the drifter trajectories reveal a well-defined, persistent westward flow along the shelf. This slope current extends from the surface to at least ~300 m depth and it is stronger during the summer months than during the winter. Temperature and salinity at 300 m were consistent with Atlantic Water. The drifter trajectories provide evidence that this current extends along the slope as far west as Herald Canyon, at least during the ice-free period.

Our annual transport estimate of 0.4 Sv at Icy Cape is similar to the 0.45 Sv estimated by Itoh et al. (2012, 2013) at the mouth of Barrow Canyon. It is, however, stronger than the annual estimate by Weingartner et al. (2017). Part of this difference can be seen in the seasonal magnitudes—in January–April both our estimate and Weingartner et al. (2017) indicated weak transport while in October–December our estimates were weakly positive, while theirs were weakly negative. The largest differences were in the summer months—our estimate of ~0.7 Sv is more in agreement with Gong and Pickart (2015) composite hydrographic estimate of 0.8 ± 0.2 Sv, than the Weingartner et al. (2017) estimate of 0.45 Sv. The discrepancies can be attributed to a variety of factors ranging from high interannual variability to failure to capture all parts of the Alaskan Coastal Current (ACC) flow, or an over-estimation of flow seaward of C3. To better estimate transport requires additional strategically placed moorings.

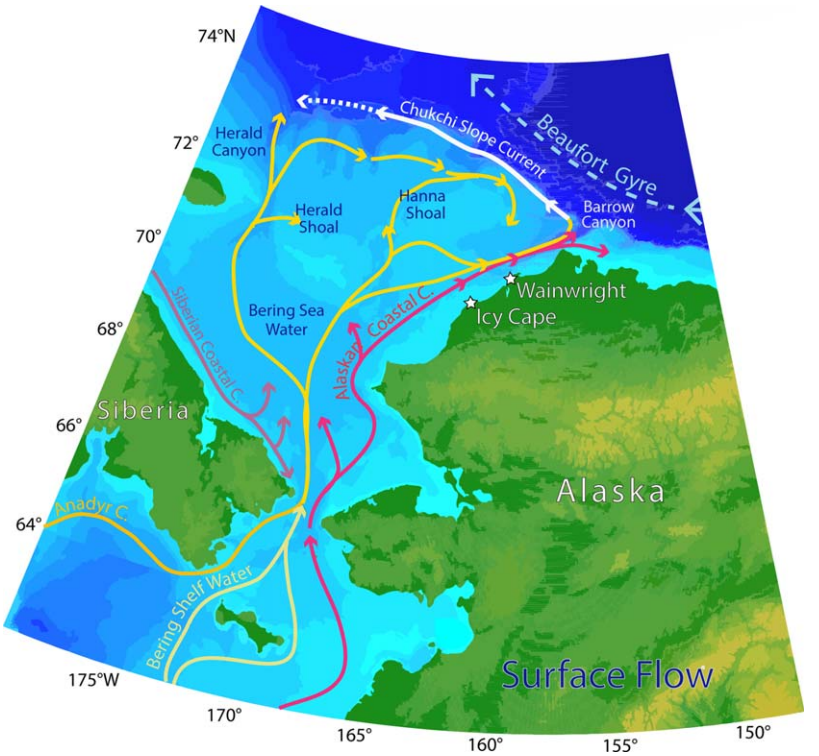

Figure 16. Composite map of various branches of the flow in the Chukchi Sea and slope. Observations from this manuscript and from two other articles (Brugler et al., 2014) are used.

The currents at C1–C6 were well correlated both horizontally and vertically, and exhibit flow that generally follows bathymetry, but with strong reversals especially evident at C1, C2, C4, and C5. These currents were well correlated with the local winds, exhibiting reversals that were associated with strong southward winds. The flow north of Hanna Shoal at C7 and C8 was weaker, poorly correlated with the currents at the other sites and poorly correlated with local winds.

All of the currents were strongly correlated in the vertical, which is not surprising given that most of the moorings (C1–C8) were in water depths of less than 50 m. One of the surprises was that the strongest mean currents (especially in the winter) were at the bottom of the water column, except at C8 where bottom currents were weaker. This is a result of two mechanisms that influence the currents on this shelf: the alongshore pressure gradient that supports northward flow along the coast, and winds, which often oppose this flow. The mean flow is northeastward, while the predominant winds are southwestward and influence the surface waters to a greater extent than the near bottom waters.

The three moorings at Icy Cape allowed the calculation of transport. There was a strong seasonal signal in transport. Annually, approximately 40% of the flow through Bering Strait passes the Icy Cape line. The percentage, however, varies seasonally with approximately half of the Bering Strait transport passing Icy Cape during June–September, and less than a fifth passing Icy Cape during December–April. This seasonal signal is a result of winds: strong northerly winds during winter disrupt the northward flowing ACC, while the weaker winds of summer have less of an effect. Note that here the ACC is used to refer to the broader region of northeastward flow, not just the area characterized by low-salinity surface waters. That the monthly transport anomalies at Icy Cape and Bering Strait are correlated is likely a result of the large-scale wind patterns.

These moorings and drifters have supplied new information of currents, transports, and their variability on the eastern Chukchi shelf, but longer time series are needed, to quantify patterns in the rapidly changing Arctic (Wood et al., 2015). These data sets will help us to identify locations for long-term moorings and thus continue collecting data to fully understand the mean currents, their variability on multiple time scales and how these might change with a changing ice environment.

Acknowledgments
We thank W. Floering and G. LeBon for deploying and recovering the moorings and D. Kachel, S. Bell, and D. Strausz, for processing the data. We thank Captain Atle Remme, F/V *Alaskan Enterprise*; Captain Fred Roman, F/V *Mystery Bay*; and Captain Kale Garcia, R/V *Aquila* (Kale Garcia), as well as all crew members. This is contribution 4388 from NOAA/PMEL, 2650 from JISAO. This research is contribution EcoFOCI-899 to NOAA's Ecosystems and Fisheries-Oceanography Coordinated Investigations. This publication is partially funded by the Joint Institute for the Study of the Atmosphere and Ocean (JISAO) under NOAA Cooperative Agreement NA10OAR4320148. We thank C. Berchok (NMML) for her leadership of CHAOZ, CHAOZ-X, and ArcWest, and Carol Fairfield and Heather Crowley (BOEM) for their endless support. Funding was provided by NOAA and the Bureau of Ocean Energy Management (BOEM) under Inter-Agency agreements M09PG00016 (CHAOZ), M12PG00021 (ArcWEST), and M13PG00026 (CHAOZ-X). The mooring data are archived with the authors and readily available upon request, they have been sent to BOEM for archive and for their use and/or distribution, and have been submitted to NOAA's National Centers for Environmental Information (NCEI). Data from 2010 to 2012 have NCEI accession 0157701 and 0149848. Data for 2013–2015 are pending and have NCEI submittal Reference ID E13NLG, 19RD6Y, 1JC625, H2LC81, UJCDN3, and 5YX626. The sea-ice data were downloaded from the National Snow and Ice Data Center (http://nsidc.org/data/g02202). Drifter data are available online (https://www.ecofoci.noaa.gov/drifters/efoci_drifterData.shtml). NCEP/NARR 3 hourly surface wind data are available through NOAA Earth System Research Laboratory (ESRL) (https://www.esrl.noaa.gov/psd/data/narr/). Woodgate's contributions to this effort were supported by National Science Foundation-AON grant PLR-1304052.

References

Aagaard, K., & Roach, A. T. (1990). Arctic ocean-shelf exchange: Measurements in Barrow Canyon. *Journal of Geophysical Research: Oceans*, *95*, 18163–18175.

Aagaard, K., Weingartner, T. J., Danielson, S. L., Woodgate, R. A., Johnson, G. C., & Whitledge, T. E. (2006). Some controls on flow and salinity in Bering Strait. *Geophysical Research Letters*, *33*, L19602. https://doi.org/10.1029/2006GL026612

Berchok, C. L., Crance, J. L., Garland, E., Mocklin, J. A., Stabeno, P. J., Napp, J. M.,. . . Clark, C. W. (2015). *Chukchi Offshore Monitoring In Drilling Area (COMIDA): Factors affecting the distribution and relative abundance of endangered whales* (Draft Final Report, OCS Study BOEM 2015-xxx). Seattle, WA: National Marine Mammal Laboratory, Alaska Fisheries Science Center, NMFS, NOAA.

Bourke, R. H., & Paquette, R. G. (1976). Atlantic water on the Chukchi shelf. *Geophysical Research Letters*, *3*, 629–632.

Brugler, E. T., Pickart, R. S., Moore, G. W. K., Roberts, S., Weingartner, T. J., & Statscewich, H. (2014). Seasonal to interannual variability of the Pacific water boundary current in the Beaufort Sea. *Progress in Oceanography*, *127*, 1–20. https://doi.org/10.1016/j.pocean.2014.05.002

Carmack, E., & Wassmann, P. (2006). Food webs and physical-biological coupling on pan-Arctic shelves: Unifying concepts and comprehensive perspectives. *Progress in Oceanography*, *71*, 446–477.

Coachman, L. K., Aagaard, K., & Tripp, R. B. (1975). *Bering Strait: The regional physical oceanography*. Seattle, WA: University of Washington Press.

Corbett, W. B., & Pickart, R. S. (2017). The Chukchi slope current. *Progress in Oceanography*, *153*, 50–65.

Danielson, S. L., Eisner, L., Ladd, C., Mordy, C., Sousa, L., & Weingartner, T. J. (2017). A comparison between late summer 2012 and 2013 water masses, macronutrients, and phytoplankton standing crops in the northern Bering and Chukchi seas. *Deep-Sea Research, Part II*, *135*, 7–26. https://doi.org/10.1016/j.dsr2.2016.05.024

Fang, Y. C., Potter, R. A., Statscewich, H., Weingartner, T. J., Winsor, P., & Irving, B. K. (2017). Surface current patterns in the northeastern Chukchi Sea and their response to wind forcing. *Journal of Geophysical Research: Oceans*, *122*, https://doi.org/10.1002/2017JC013121

Garrison, G. R., & Becker, P. (1976). The Barrow Submarine Canyon: A drain for the Chukchi Sea. *Journal of Geophysical Research*, *81*, 4445–4453.

Gong, D., & Pickart, R. S. (2015). Summertime circulation in the eastern Chukchi Sea. *Deep-Sea Research, Part II*, *118*, 18–31. https://doi.org/10.1016/j.dsr2.2015.02.006

Itoh, M., Nishino, S., Kawaguchi, Y., & Kikuchi, T. (2013). Barrow Canyon volume, heat, and freshwater fluxes revealed by long-term mooring observations between 2000 and 2008. *Journal of Geophysical Research: Oceans*, *118*, 4363–4379. https://doi.org/10.1002/jgrc.20290

Itoh, M., Shimada, K., Kamoshida, T., McLaughlin, F., Carmack, E., & Nishino, S. (2012). Interannual variability of Pacific Winter Water inflow through Barrow Canyon from 2000 to 2006. *Journal of Oceanography*, *68*, 575–592.

Kinder, T. H., Chapman, D. C., & Whitehead, J. A. Jr. (1986). Westward intensification of the mean circulation on the Bering Sea shelf. *Journal of Physical Oceanography*, *16*, 1217–1229.

Ladd, C., & Bond, N. A. (2002). Evaluation of the NCEP/NCAR reanalysis in the NE Pacific and the Bering Sea. *Journal of Geophysical Research: Oceans*, *107*(C10), 3158. https://doi.org/10.1029/2001JC001157

Ladd, C., Mordy, C. W., Salo, S. A., & Stabeno, P. J. (2016). Winter water properties and the Chukchi polynya. *Journal of Geophysical Research: Oceans*, *121*, 5516–5534. https://doi.org/10.1002/2016JC011918

Martin, T., Steele, M., & Zhang, J. (2014). Seasonality and long-term trend of Arctic Ocean surface stress in a model. *Journal of Geophysical Research: Oceans*, *119*, 1723–1738. https://doi.org/10.1002/2013JC009425

Mesinger, F., DiMego, G., Kalnay, E., Mitchell, K., Shafran, P. C., Ebisuzaki, W.,. . . Shi, W. (2006). North American regional reanalysis. *Bulletin of the American Meteorological Society*, *87*(3), 343–360. https://doi.org/10.1175/bams-87-3-343

Mountain, D. G., Coachman, L. K., & Aagaard, K. (1976). On the flow through Barrow Canyon. *Journal of Physical Oceanography*, *6*, 461–470.

Paquette, R. G., & Bourke, R. H. (1974). Observations on the coastal current of arctic Alaska. *Journal of Marine Research*, *32*, 195–207.

Pickart, R. S., Pratt, L. J., Torres, D. J., Whitledge, T. E., Proshutinsky, A. Y., Aagaard, K.,. . . Dail, H. J. (2010). Evolution and dynamics of the flow through Herald Canyon in the western Chukchi Sea. *Deep-Sea Research, Part II*, *57*(1–2), 5–26. https://doi.org/10.1016/j.dsr2.2009.08.002

Pickart, R. S., Spall, M. A., Moore, G. W. K., Weingartner, T. J., Woodgate, R. A., Aagaard, K., & Shimada, K. (2011). Upwelling in the Alaskan Beaufort Sea: Atmospheric forcing and local versus non-local response. *Progress in Oceanography*, *88*(1–4), 78–100. https://doi.org/10.1016/j.pocean.2010.11.005

Schumacher, J. D., Stabeno, P. J., & Roach, A. T. (1989). Volume transport in the Alaska Coastal Current. *Continental Shelf Research*, *9*(12), 1071–1083.

Stabeno, P. J., Bell, S., Cheng, W., Danielson, S., Kachel, N. B., & Mordy, C. W. (2016). Long-term observations of Alaska Coastal Current in the northern Gulf of Alaska. *Deep-Sea Research, Part II*, *132*, 24–40. https://doi.org/10.1016/j.dsr2.2015.12.016

Stabeno, P. J., & Hristova, H. G. (2014). Observations of the Alaskan Stream near Samalga Pass and its connection to the Bering Sea: 2001–2004. *Deep-Sea Research, Part I*, *88*, 30–46. https://doi.org/10.1016/j.dsr.2014.03.002

Stabeno, P. J., Reed, R. K., & Schumacher, J. D. (1995). The Alaska Coastal Current: Continuity of transport and forcing. *Journal of Geophysical Research: Oceans*, *100*, 2477–2485.

Stigebrandt, A. (1984). The North Pacific: A global-scale estuary. *Journal of Physical Oceanography*, *14*, 464–470. https://doi.org/10.1175/1520-0485(1984)014<0464:TNPAGS>2.0.CO;2

Weingartner, T., Aagaard, K., Woodgate, R., Danielson, S., Sasaki, Y., & Cavalieri, D. (2005). Circulation on the north central Chukchi Sea shelf. *Deep-Sea Research, Part II*, *52*(24–26), 3150–3174. https://doi.org/10.1016/j.dsr2.2005.10.015

Weingartner, T., Dobbins, E., Danielson, S., Winsor, P., Potter, R., & Statscewich, H. (2013). Hydrographic variability over the northeastern Chukchi Sea shelf in summer-fall 2008–2010. *Continental Shelf Research*, *67*, 5–22. https://doi.org/10.1016/j.csr.2013.03.012

Weingartner, T. J., Potter, R. A., Stoudt, C. A., Dobbins, E. L., Statscewich, H., Winsor, P. R.,. . . Borg, K. (2017). Transport and thermohaline variability in Barrow Canyon on the northeastern Chukchi Sea Shelf. *Journal of Geophysical Research: Oceans*, *122*, 3565–3585. https://doi.org/10.1002/2016JC01263

Wood, K. R., Bond, N. A., Danielson, S. L., Overland, J. E., Salo, S. A., Stabeno, P., & Whitefield, J. (2015). A decade of environmental change in the Pacific-Arctic region, *Progress in Oceanography*, *136*, 12–31. https://doi.org/10.1016/j.pocean.2015.05.005

Woodgate, R. A., & Aagaard, K. (2005). Revising the Bering Strait freshwater flux into the Arctic Ocean. *Geophysical Research Letters*, *32*, L02602. https://doi.org/10.1029/2004GL021747

Woodgate, R. A., Aagaard, K., & Weingartner, T. J. (2005a). Monthly temperature, salinity, and transport variability of the Bering Strait through flow. *Geophysical Research Letters*, *32*, L04601. https://doi.org/10.1029/2004GL021880

Woodgate, R. A., Aagaard, K., & Weingartner, T. J. (2005b). A year in the physical oceanography of the Chukchi Sea: Moored measurements from autumn 1990–1991. *Deep-Sea Research, Part II*, *52*(24–26), 3116–3149. https://doi.org/10.1016/j.dsr2.2005.10.016

Woodgate, R. A., Stafford, K. M., & Prahl, F. G. (2015). A synthesis of year-round interdisciplinary mooring measurements in the Bering Strait (1990–2014) and the RUSALCA years (2004–2011). *Oceanography*, *28*(3), 46–67. https://doi.org/10.5670/oceanog.2015.57

Woodgate, R. A., Weingartner, T. J., & Lindsay, R. W. (2010). The 2007 Bering Strait oceanic heat flux and anomalous Arctic Sea-ice retreat. *Geophysical Research Letters*, *37*, L01602. https://doi.org/10.1029/2009GL041621

Woodgate, R. A., Weingartner, T. J., & Lindsay, R. (2012). Observed increases in Bering Strait oceanic fluxes from the Pacific to the Arctic from 2001 to 2011 and their impacts on the Arctic Ocean water column. *Geophysical Research Letters*, *39*, L24603. https://doi.org/10.1029/2012GL054092